OPEN ACCESS
IOP Publishing
Plasma Sources Science and Technology
Plasma Sources Sci. Technol. **28** (2019) 095024 (10pp)
https://doi.org/10.1088/1361-6595/ab2d6b

Electron energy loss spectroscopy of wall charges in plasma-facing dielectrics

E Thiessen, F X Bronold[1] and H Fehske

Institut für Physik, Universität Greifswald, 17489 Greifswald, Germany

E-mail: bronold@physik.uni-greifswald.de

Received 30 January 2019, revised 2 June 2019
Accepted for publication 27 June 2019
Published 24 September 2019

Abstract

We propose a setup enabling electron energy loss spectroscopy to determine the density of the electrons accumulated by an electropositive dielectric in contact with a plasma. It is based on a two-layer structure inserted into a recess of the wall. Consisting of a plasma-facing film made out of the dielectric of interest and a substrate layer, the structure is designed to confine the plasma-induced surplus electrons to the region of the film. The charge fluctuations they give rise to can then be read out from the backside of the substrate by near specular electron reflection. To obtain in this scattering geometry a strong charge-sensitive reflection maximum due to the surplus electrons, the film has to be most probably pre-n-doped and sufficiently thin with the mechanical stability maintained by the substrate. Taking electronegative CaO as a substrate layer we demonstrate the feasibility of the proposal by calculating the loss spectra for Al_2O_3, SiO_2, and ZnO films. In all three cases we find a reflection maximum strongly shifting with the density of the surplus electrons and suggest to use it for charge diagnostics.

Keywords: electron energy loss spectroscopy, surface double layer, plasma sheaths

1. Introduction

The most fundamental manifestation of the interaction of a plasma with a solid is the formation of an electric double layer consisting, respectively, of an electron-depleted and electron-rich space charge region on the plasma and the solid side of the interface [1]. It arises because electrons are deposited more efficiently onto or into the surface, depending on its electronic structure, than they are extracted from it by neutralization/de-excitation of ions/radicals [2]. Since the beginning of gaseous electronics [3] it has been known that an electric double layer is formed at plasma-solid interfaces. Yet a microscopic understanding of the solid-based part of the double layer is still missing, mostly because of the limitations of the diagnostics for surface charges and because it was so far–perhaps–not essential for the success of plasma physics and technology. Continuing progress in the miniaturization of integrated microdischarges [4, 5], however, driven by the desire to combine solid-state and gaseous electronics [6, 7], makes the embracing solid structure an integral part of the plasma-device. In these structures the solid- and plasma-based charge dynamics are intimately linked. A complete understanding of the discharge requires thus an upgrade to plasma diagnostics using techniques which also provide a view on the charge dynamics inside the plasma-facing solid. Even technological plasma applications would benefit from such diagnostics. For instance, plasma catalysis [8] often involves charge-transfer across a plasma-solid interface. Having an in-operando view on it would foster the investigation of the elementary quantum-mechanical processes underlying the surface chemistry in a plasma environment.

There exists a number of techniques to estimate the charge accumulated by plasma-facing solids. Electric probes [9], surface potential measurements [10–12], opto-mechanical devices based on the reflection of a laser by a cantilever [13], and the Pockels effect of an electro-optic crystal [14–19] have been employed for that purpose. However, with the exception of the Pockels effect measurements, the methods are rather invasive. In addition, they are limited to measuring the total charge accumulated by the plasma-facing solid. How the

[1] Author to whom any correspondence should be addressed.

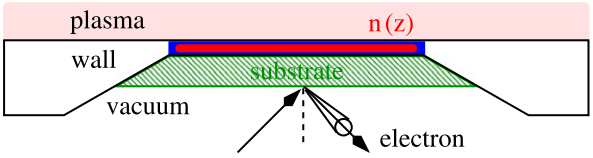

Figure 1. Illustration (not on scale) of the proposed setup for measuring the plasma-induced wall charge by electron energy loss spectroscopy. The idea is to confine the wall charge $n(z)$ in a thin film, stabilize it using a substrate, and read out the charge information with an electron beam applied from the backside.

charge is distributed normal to the plasma-wall interface cannot be determined. Information about the charge dynamics inside the solid can also not be obtained by these methods.

To overcome the limitations of the existing methods we recently proposed infrared attenuated reflection (IR-ATR) spectroscopy as a tool for gaining access to the surplus charges in a dielectric exposed to a plasma [20]. The proposal relies on a layered structure supporting a Berreman mode in the infrared which turns out to be rather charge-sensitive. Combined with a self-consistent description of the electric double layer at the plasma-solid interface the method has the potential to provide not only the total charge deposited into the solid (which we demonstrated by an exploratory calculation [20]) but also its spatial distribution inside the solid.

Another experimental technique of solid state physics–electron energy loss spectroscopy (EELS) (see [21–26] for a general introduction)–could be perhaps also used as a diagnostic for the electrons accumulated by a plasma-facing solid. EELS is an electron reflection technique where the probing electron couples to the dipole fields of the charge fluctuations inside the solid. As a result it loses energy as well as momentum and scatters a bit off the specular direction. The cross section for the near specular reflection thus contains information about charge fluctuations inside the solid. An asset of EELS is that it is an electron spectroscopy technique. The spatial resolution is thus ultimately given by the de Broglie wavelength of the probing electron. Even taking instrumental limitations into account, it will be much better than for any other technique employed so far for surface charge measurements.

In a number of experiments it was shown that EELS can be used to determine parameters characterizing the inhomogeneous electron gases formed at semiconductor surfaces [27–31]. If it were not for the fact that the plasma prevents applying the probing electron beam directly to the plasma-solid interface it would be clear that EELS can be used as a wall charge diagnostics in plasma applications. To enable EELS to measure the charge accumulated by a plasma-facing solid, an indirect setup has to be used. It is the purpose of this paper to describe such a setup and to demonstrate using a model calculation its feasibility as a testbed for investigating the charging of solids exposed to a plasma.

As a first step we focus on a setup measuring the total charge accumulated by an electropositive dielectric in contact with a plasma, leaving modifications required for an analysis of the depth profile for future work. The setup is shown in figure 1. It consists of a two-layer structure inserted into a recess of the wall. Within the structure a film made out of the dielectric of interest is in contact with the plasma and supported by a substrate layer. The electron beam supposed to read out the charge information is applied from the side opposite to the plasma-solid interface. Interference with the plasma is thus excluded on the expense of using a thin film structure. For the setup to work it has to be designed in a particular manner. Our calculations indicate the probing electron beam to be sensitive to the fluctuations of the plasma-induced surplus electrons in the film if the thickness of the whole structure is in the sub-100 nm range. In addition we found it advantageous to confine the surplus electrons coming from the plasma to the region of the film by the line-up of the conduction band edges of the film and the substrate. To compensate for the loss of signal strength due to the substrate we suggest moreover to pre-n-dope the plasma-facing film. The last measure is not of principal importance. It is only required for making the signal detectable with EELS instrumentation currently available.

The outline of the rest of the paper is as follows. In the next section we calculate the cross section for near specular electron reflection from a two-layer structure in contact with a plasma. Due to the confinement of the charge to a thin film the de Broglie wavelength of the electrons is on the same order as the screening length, forcing us to employ the nonlocal response theory of Mills and coworkers [32–34]. Numerical results for an Al_2O_3, an SiO_2, and a ZnO film, respectively, on top of a CaO layer, which are material combinations meeting the requirements listed above, are then presented in section 3. For film thicknesses in the order of a few 10s of nanometers and background dopings in the order of 10^{18} cm^{-3} we find a maximum in the reflection cross section due to the collective excitation of the total number of electrons in the film which is sufficiently strong to be detectable and charge-sensitive to serve as a diagnostic for the density of the film's surplus electrons coming from the plasma. Section 4 concludes the presentation by summarizing its main points.

2. Theoretical background

We consider EELS in an unusual geometry where the probing electron approaches a layered structure of finite width from the side opposite to the interface of interest, which–in our case–is the interface between a plasma and an uppermost layer of a stack of materials. As illustrated in figure 2, the structure and its embedding are characterized by a set of dielectric functions ε_i with $i = v, s, f, p$ and a potential profile $V_{\mathrm{conf}}(z)$ accounting for the offsets of the layer's conduction band edges from the potential just outside the structure (electron affinities χ). The energy loss we want to detect and use as a charge diagnostic arises from the density $n(z)$ of electrons accumulated in the film next to the plasma. For simplicity we characterize the plasma using a dielectric function ε_p which we moreover set at the end to ε_v, thereby neglecting charge fluctuations inside the plasma. To take them into account is beyond the scope of the present work; however it constitutes no principal problem.

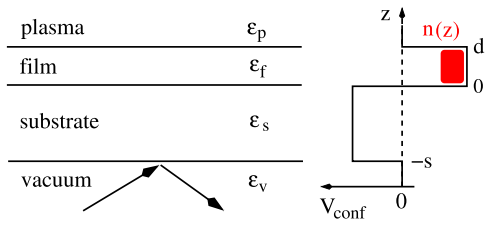

Figure 2. Geometry of the structure we investigated. It consists of an electropositive film with thickness d and an electronegative substrate with thickness s embedded between a plasma and a vacuum. The layers as well as the plasma and the vacuum are characterized by background dielectric functions ε_i with $i = p, f, s, v$ as indicated and the electron beam is applied from the vacuum side. On the right is plotted the potential profile confining electrons to the region of the film. It arises from the positive and negative electron affinities χ of the film and the substrate, respectively, and is essential for the operation of the charge measuring device we propose.

2.1. Cross section for EELS

Using the coordinate system of figure 2 and assuming charge fluctuations to arise solely from the stack of materials, the microscopic approach developed by Mills [32] gives for the momentum-integrated EELS cross section

$$\frac{\mathrm{d}S}{\mathrm{d}\omega} = \frac{2e^2}{\pi\hbar}|R_I|^2 \int_D \mathrm{d}^2q_\parallel R(\vec{q}_\parallel, \omega) P(\vec{q}_\parallel, \omega), \tag{1}$$

where $|R_I|^2$ is the probability for quantum-mechanical reflection from the vacuum-substrate interface, which we set to unity in the following, the surface-rider function

$$R(\vec{q}_\parallel, \omega) = \frac{v_\perp^2}{[v_\perp^2 q_\parallel^2 + (\omega - \vec{v}_\parallel \cdot \vec{q}_\parallel)^2]^2}, \tag{2}$$

accounting for the scattering kinematics, where $\vec{v}_\parallel$ and $\vec{v}_\perp$ are the electron's velocity components parallel and perpendicular to the surface, and the loss function ($a = |\vec{a}|$ for any vector $\vec{a}$)

$$P(\vec{q}_\parallel, \omega) = \frac{e^2}{\hbar}\int \mathrm{d}^2x_\parallel \int_{-\infty}^{\infty} \mathrm{d}t\ e^{\mathrm{i}\vec{q}_\parallel\cdot\vec{x}_\parallel - \mathrm{i}\omega t} \int_{-s}^{d} \mathrm{d}z \times \int_{-s}^{d} \mathrm{d}z' e^{-q_\parallel(z+z'+2s)} \langle \delta\rho^\dagger(\vec{x}_\parallel, z'; t)\delta\rho(0, z; 0)\rangle_T, \tag{3}$$

taking the transfer of energy $\hbar\omega$ and lateral momentum $\vec{q}_\parallel$ parallel to the xy-plane from the electron to the solid structure into account. It forces the outgoing branch of the scattering trajectory to deviate a little from the specular direction and therefore carries the information we are looking for.

To the EELS signal not all lateral momenta $\vec{q}_\parallel$ contribute. Switching to cylindrical coordinates with the polar angle ϕ measured with respect to $\vec{v}_\parallel$, one realizes that the integration domain D relevant for EELS is bounded by the ellipse equation [22]

$$\frac{1}{[q_\parallel^c(\phi)]^2} = \frac{\sin^2(\phi)}{[q_\parallel^{\max}]^2} + \frac{\cos^2(\phi)}{[q_\parallel^{\max}\cos(\phi_i)]^2}, \tag{4}$$

where ϕ_i is the incident angle of the probing beam with respect to the surface normal, $q_\parallel^{\max} = q_{\mathrm{dB}}\phi_a$, $q_{\mathrm{dB}} = \sqrt{2E_0 m}/\hbar$ is the de Broglie wavenumber of the scattering electron incoming with energy E_0 and ϕ_a is half of the acceptance angle of the detector.

The essential part of the cross section is the loss function $P(\vec{q}_\parallel, \omega)$ which via (3) is related to the charge-charge correlation function $\langle \delta\rho^\dagger(\vec{x}_\parallel, z', t)\delta\rho(0, z, 0)\rangle_T$, where the operator $\delta\rho(\vec{x}_\parallel, z', t)$ describes the charge fluctuations arising in the spatial region for which $-s < z < d$ and the brackets denote the thermodynamical average taken over this domain at temperature T. Clearly this is an approximation. It assumes that the plasma-facing structure is in thermal equilibrium. In reality this is not the case, but at this early stage of exploring EELS as a charge diagnostic the equilibrium assumption seems justified. Including the non-equilibrium aspects would unnecessarily mask the basic idea we want to convey and will be the subject of future work.

From the integrand in (3) arises a problem for the from-the-back detection of the EELS signal. Because of the substrate layer the absolute value of the argument of the exponential function is even in the most favorite situation $q_\parallel s$, with s being the thickness of the substrate, and [29]

$$q_\parallel \simeq \sqrt{\frac{2m_e}{\hbar^2}}\frac{\hbar\omega\sin\phi_i}{2\sqrt{E_0}} \tag{5}$$

being the momentum transferred from the electron to the solid; $\hbar\omega$ is the energy of the charge fluctuation to be detected and m_e is the electron mass. Compared to a system without a substrate the EELS signal is hence suppressed by a factor of $\exp(-q_\parallel s)$ implying for $s \simeq q_\parallel^{-1}$ the intensity to be decreased by roughly 37%. Thin substrates are thus required for strong signals but they have to be also mechanically stable, limiting in practice how thin they can be.

2.2. Charge fluctuations

We are interested in the EELS fingerprint of the electrons residing in the plasma-facing film. To identify their contribution to (1) we have to isolate the film's electronic charge fluctuation $\delta\rho_e$ from the total charge fluctuation $\delta\rho$ of the two-layer structure. An elegant scheme to accomplish this, due originally to Ehlers and Mills [33], who used it to describe EELS from space charge regions at semiconductor surfaces, is based on a consideration of the potential fluctuations outside the solid probed by the EELS electron; subsequently Streight and Mills [34] applied it also to EELS from semiconducting films. Adopted to our situation the potential fluctuations in the region $z < -s$ arising from the charge fluctuations in the region $z > -s$ have to be calculated. On the one hand, this can be done by using the general expression for the electric potential and expanding the factor $|\vec{x} - \vec{x}'|^{-1}$ in terms of surface waves [21]. It can however be also obtained by solving, for a point charge located in the film, the Poisson equation with boundary conditions appropriate for the two-layer structure under consideration. Weighting the result with the distribution $\delta\rho_e(\vec{q}_\parallel, z, t)$ of surplus electrons in the film gives then an alternative expression for the potential fluctuations which via comparison with the former allows one to relate $\delta\rho_e(\vec{q}_\parallel, z, t)$ to $\delta\rho(\vec{q}_\parallel, z, t)$.

The first approach, based on the general expression for the electric potential in front of the stack, leads to

$$\delta\Phi(\vec{x}, t) = \int \frac{\mathrm{d}^2 q_\parallel}{(2\pi)^2} e^{i\vec{q}_\parallel \cdot \vec{x}_\parallel} \delta\Phi(\vec{q}_\parallel, z, t) \tag{6}$$

with $z < -s$ and

$$\delta\Phi(\vec{q}_\parallel, z, t) = \frac{2\pi e}{q_\parallel} \int_{-s}^{d} \mathrm{d}z' e^{q_\parallel (z-z')} \delta\rho(\vec{q}_\parallel, z', t). \tag{7}$$

The imbedding strategy, on the other hand, working with the Poisson equation, given

$$\nabla \cdot [\varepsilon(z) \nabla \Phi(\vec{x})] = -4\pi e \delta(x') \delta(y') \delta(z' - z), \tag{8}$$

where the point charge is located at $x' = y' = 0$ and $d > z' > 0$, that is, inside the film, yields upon utilizing the homogeneity in the xy-plane,

$$\Phi(\vec{x}) = \int \frac{\mathrm{d}^2 q_\parallel}{(2\pi)^2} e^{i\vec{q}_\parallel \cdot \vec{x}_\parallel} \Phi(q_\parallel, z) \tag{9}$$

with

$$\Phi(q_\parallel, z) = A e^{q_\parallel z} + B e^{-q_\parallel z} \tag{10}$$

and expansion coefficients A and B determined from the boundary conditions appropriate for the z-dependent dielectric function

$$\varepsilon(z) = \begin{cases} \varepsilon_v & \text{for} \quad z < -s \\ \varepsilon_s & \text{for} \quad -s < z < 0 \\ \varepsilon_f & \text{for} \quad 0 < z < d \\ \varepsilon_p & \text{for} \quad z > d \end{cases}. \tag{11}$$

For the imbedding strategy to be applicable the imaginary parts of the dielectric functions ε_i have to be of course negligible in the frequency range of interest. Enforcing the boundary conditions,

$$\Phi(q_\parallel, z^-) = \Phi(q_\parallel, z^+) \tag{12}$$

$$\varepsilon(z^-) \frac{\mathrm{d}\Phi(q_\parallel, z)}{\mathrm{d}z}\bigg|_{z^-} - \varepsilon(z^+) \frac{\mathrm{d}\Phi(q_\parallel, z)}{\mathrm{d}z}\bigg|_{z^+} = \begin{cases} 4\pi e & \text{if} \quad z = z' \\ 0 & \text{else} \end{cases} \tag{13}$$

at $z = -s$, $z = 0$, and $z = d$ and setting $B = 0$ for $z < -s$ and $A = 0$ for $z > d$ we find–after weighting the result with the (instantaneous) charge distribution inside the film and Fourier transforming the lateral spatial variables–for the potential in the region $z < -s$, denoted now again by $\delta\Phi(\vec{q}_\parallel, z, t)$, the expression

$$\delta\Phi(\vec{q}_\parallel, z, t) = \frac{(2\pi e/q_\parallel) 4\varepsilon_s}{(\varepsilon_f + \varepsilon_s)(\varepsilon_s + \varepsilon_v) h(q_\parallel; \varepsilon_s, s; \varepsilon_f, d; \varepsilon_p, \varepsilon_v)} \times \int_{-s}^{d} \mathrm{d}z' e^{q_\parallel (z-z')} F(q_\parallel, z'; \varepsilon_f, d; \varepsilon_p) \delta\rho_e(\vec{q}_\parallel, z', t) \theta(z'), \tag{14}$$

with the auxiliary functions

$$h(q_\parallel; \varepsilon_s, s; \varepsilon_f, d; \varepsilon_p, \varepsilon_v) = 1 + L_{sv} L_{fs} e^{-2q_\parallel s} - L_{fp} L_{fs} e^{-2q_\parallel d} - L_{fp} L_{sv} e^{-2q_\parallel (d+s)} \tag{15}$$

and

$$F(q_\parallel, z; \varepsilon_f, d; \varepsilon_p) = 1 + L_{fp} e^{-2q_\parallel (d-z)}, \tag{16}$$

where

$$L_{ij} = \frac{\varepsilon_i - \varepsilon_j}{\varepsilon_i + \varepsilon_j} \quad \text{with} \quad i, j = v, s, f, p. \tag{17}$$

Comparison of (7) and (14) yields then a relation between $\delta\rho(\vec{q}_\parallel, z', t)$ and $\delta\rho_e(\vec{q}_\parallel, z', t)$ which when inserted into (3) leads, after some algebra, to the loss function

$$P(\vec{q}_\parallel, \omega) = 2e^2 (1 + n(\omega)) \times \left[\frac{4\varepsilon_s}{(\varepsilon_f + \varepsilon_s)(\varepsilon_s + \varepsilon_v) h(q_\parallel; \varepsilon_s, s; \varepsilon_f, d; \varepsilon_p)} \right]^2 \times \int_0^d \mathrm{d}z \int_0^d \mathrm{d}z' e^{-q_\parallel (z + z' + 2s)} F(q_\parallel, z; \varepsilon_f, d; \varepsilon_p) \times F(q_\parallel, z'; \varepsilon_f, d; \varepsilon_p) \mathrm{Im}\chi(\vec{q}_\parallel, \omega; z, z') \tag{18}$$

with $n(\omega)$ the Bose distribution function with $\beta = 1/(k_B T)$ and

$$\chi(\vec{q}_\parallel, \omega; z, z') = \frac{i\theta(\omega)}{\hbar} \langle [\delta\rho_e^\dagger(\vec{q}_\parallel, z, \omega), \delta\rho_e(\vec{q}_\parallel, z', 0)] \rangle_T \tag{19}$$

the (commutator) density-density response function for the surplus electrons [33, 34]. The calculation of the loss function $P(\vec{q}_\parallel, \omega)$ has thus been reduced to the determination of the function $\chi(\vec{q}_\parallel, \omega; z, z')$. The fact that the electrons are embedded in a dielectric structure is taken into account in (18) by the functions in front of $\mathrm{Im}\,\chi(\vec{q}_\parallel, \omega; z, z')$.

2.3. Density-density response function

The simplest scheme for obtaining the density-density response function $\chi(\vec{q}_\parallel, \omega; z, z')$ relies on the random-phase approximation. As in the work of Mills and coworkers [33, 34] it is based on the integral equation

$$\chi(\vec{q}_\parallel, \omega; z, z') = \chi_0(\vec{q}_\parallel, \omega; z, z') - \int_0^d \mathrm{d}z'' K(\vec{q}_\parallel, \omega; z, z'') \chi(\vec{q}_\parallel, \omega; z'', z'), \tag{20}$$

where the kernel

$$K(\vec{q}_\parallel, \omega; z, z') = \int_0^d \mathrm{d}z'' \chi_0(\vec{q}_\parallel, \omega; z, z'') v(q_\parallel; z'', z') \tag{21}$$

includes the electron-electron interaction $v(q_\parallel; z, z')$ and the irreducible particle-hole propagator $\chi_0(\vec{q}_\parallel, \omega; z, z')$. Writing for the interaction potential $v(q_\parallel; z, z') = e\Phi(q_\parallel, z, z')$, with $\Phi(q_\parallel, z, z')$ the electric potential at z induced by a point charge at z', where both z and z' are inside the film, the solution of the Poisson equation (8) can be utilized to deduce

$$v(q_\parallel; z, z') = \frac{2\pi e^2}{q_\parallel \varepsilon_f} \frac{g(q_\parallel; \varepsilon_s, s; \varepsilon_f, d; \varepsilon_p, \varepsilon_v)}{h(q_\parallel; \varepsilon_s, s; \varepsilon_f, d; \varepsilon_p, \varepsilon_v)} \tag{22}$$

where

$$g(q_\parallel;\,\varepsilon_s,\,s;\,\varepsilon_f,\,d;\,\varepsilon_p,\,\varepsilon_v) = e^{-q_\parallel|z-z'|} + L_{sv}e^{-q_\parallel(z+z'+2s)} + L_{fs}e^{-q_\parallel(z+z')} + L_{fp}e^{-q_\parallel(2d-(z+z'))} + L_{sv}L_{fs}e^{-q_\parallel(2s+|z-z'|)} + L_{sv}L_{fp}e^{-q_\parallel(2(s+d)-|z-z'|)} + L_{fs}L_{fp}e^{-q_\parallel(2d-|z-z'|)} + L_{sv}L_{fs}L_{fp}e^{-q_\parallel(2(d+s)-(z+z'))}. \tag{23}$$

To complete the construction of the kernel (21) we also need the irreducible electron-hole propagator $\chi_0(\vec{q}_\parallel,\,\omega;\,z,\,z')$. It is given by [33, 34]

$$\chi_0(\vec{q}_\parallel,\,\omega;\,z,\,z') = \frac{2}{A}\sum_{\vec{k}_\parallel}\sum_{i,j}\frac{f(\vec{k}_\parallel,\,i) - f(\vec{k}_\parallel+\vec{q}_\parallel,\,j)}{\hbar\omega + \mathrm{i}\delta + E_{\vec{k}_\parallel} - E_{\vec{k}_\parallel+\vec{q}_\parallel,j}} \times \psi_i^*(z)\psi_i(z')\psi_j(z)\psi_j^*(z'), \tag{24}$$

where

$$f(\vec{k}_\parallel,\,i) = \frac{1}{e^{\beta(E_{\vec{k}_\parallel,i}-\mu)}+1} \tag{25}$$

is the Fermi distribution function with $\beta = 1/(k_BT)$ and μ is the chemical potential; A is the quantization area in the xy-plane.

The single electron energies entering (24) contain the energy of the lateral and the vertical motion,

$$E_{\vec{k}_\parallel,i} = \frac{\hbar^2k_\parallel^2}{2m^*} + \varepsilon_i \tag{26}$$

with the energy ε_i belonging to $\psi_i(z)$, the part of the wavefunction describing the perpendicular motion. To obtain ε_i and $\psi_i(z)$ we assume the film to constitute an infinitely deep potential well. Both quantities can then be looked up in textbooks about quantum mechanics [35]. It is thus not necessary to list them here. Since the electron affinities of Al_2O_3, SiO_2, and ZnO, the materials we will take for the film, are large and positive, the infinitely deep quantum well is a reasonable approximation. Improvements are possible but will be not addressed in this paper. The labels i, j are the quantum numbers labeling the eigenstates of the well and δ is a small but finite number preventing numerical instability. For the results discussed in the next section $\delta = 10^{-5}$. Finally, the chemical potential μ has to be determined. It is related to the surface charge density through the condition [36]

$$n_s = \frac{m^*}{\pi\hbar^2\beta}\sum_i \ln(1 + e^{-\beta(\varepsilon_i-\mu)}). \tag{27}$$

Inside the film the electrons are distributed according to

$$n(z) = \frac{m^*}{\pi\hbar^2\beta}\sum_i \ln(1 + e^{-\beta(\varepsilon_i-\mu)})|\psi_i(z)|^2, \tag{28}$$

which after integration over z yields (27), as it should, because of the normalization of the wavefunctions.

2.4. Remarks concerning the numerics

The numerical work consists of two major parts: (i) calculating the density-density response function $\chi(\vec{q}_\parallel,\,\omega;\,z,\,z')$ by solving the integral equation (20) and (ii) integrating $\chi(\vec{q}_\parallel,\,\omega;\,z,\,z')$ over z and z' as specified in (18) to obtain the loss function $P(\vec{q}_\parallel,\,\omega)$, which is then inserted into (1) to yield after integrating over $\vec{q}_\parallel$ the EELS cross section $dS/d\omega$.

In order to obtain $\chi(\vec{q}_\parallel,\,\omega;\,z,\,z')$ we first have to construct the function $\chi_0(\vec{q}_\parallel,\,\omega;\,z,\,z')$. For that purpose we closely follow Ehlers and Mills [33] and adopt their approach to the layered structure we consider. Hence, we convert the summation over $\vec{k}_\parallel$ to an integral and rewrite (24) using Green functions. Only one sum over the eigenstate labels i remains then. Due to the homogeneity in the xy-plane it turns out that all quantities depend only on the absolute value of $\vec{q}_\parallel$ which is chosen parallel to the x-direction. For the solution of the integral equation (20) itself we no longer follow Ehlers and Mills [33]. Instead we employ the numerical strategy Streight and Mills [34] used in their study of semiconducting films. They noticed that for a film the numerical work can be greatly reduced by integrating out the variable z' which enters (20) and (18) only as a parameter. Instead of solving (20) for $\chi(q_\parallel,\,\omega;\,z,\,z')$, depending as we now know only on $q_\parallel$, we thus solve an integral equation for

$$X(q_\parallel,\,\omega;\,z) = \int_0^d \mathrm{d}z' F(q_\parallel,\,z';\,\varepsilon_f,\,d;\,\varepsilon_p)e^{-q_\parallel z'}\chi(q_\parallel,\,\omega;\,z,\,z'), \tag{29}$$

which can be easily derived from (20) and efficiently solved by discretization and matrix inversion.

Obtaining $\chi(q_\parallel,\,\omega;\,z,\,z')$ in the manner described is numerically the most challenging task. The integrations specified in (1) and (18), on the other hand, can be performed with standard integration routines. For the numerical work we used dimensionless variables, measuring energies and lengths, respectively, in units of k_BT and $\lambda_* = \sqrt{\hbar^2/2m_e^*k_BT}$, where m_e^* is the effective electron mass in the conduction band of the film.

3. Results

We now present results for our setup, taking a layer of CaO as a substrate to which an electron beam is applied from below with energy $E_0 = 5$ eV and angle of incidence $\phi = 45°$. The acceptance angle of the electron detector is $2\phi_a = 2°$ and the films on top of the substrate facing the plasma are made out of Al_2O_3, SiO_2, and ZnO.

The materials meet the criteria we impose for the setup to work as a testbed for measuring the wall charge of electropositive dielectrics and also for our theory to be applicable: (i) charge confinement to the film, (ii) dielectric functions with small imaginary parts in the spectral range of interest, and (iii) mechanical stability. Al_2O_3, SiO_2, and ZnO, are electropositive dielectrics with electron affinities $\chi = 2.58$ eV [42], 1.3 eV [43], and 4.1 eV [44], whereas CaO is electronegative

with $\chi = -0.86$ eV [45]. Hence, the surplus electrons coming from the plasma will be confined to the films. In the energy range of the charge fluctuation we probe using EELS, the imaginary parts of the dielectric functions are moreover very small. The argument enabling us to express the total charge fluctuation as a product of a factor describing the background and a factor describing the surplus electrons is thus justified. Finally, the mechanical properties of the materials make them suitable for our setup. Their microhardnesses, for instance, are on the same order as the one for Si_3N_4 which is used as a sub-100nm membrane to withstand pressure gaps at vacuum-liquid [46] as well as vacuum-plasma interfaces [47, 48] in various types of from-the-back microscopies. We expect therefore Al_2O_3, SiO_2, ZnO, and CaO to allow the construction of sub-100nm film-substrate structures required for the EELS measurements we propose. Si_3N_4 itself cannot be used for two reasons: first, it is electropositive. Only with hydrogen adlayers may it become electronegative [49], which adds an additional complexity to the setup. Second, in the spectral range of interest the dielectric function of Si_3N_4 has a large imaginary part damping out the EELS signal and making also our image charge construction inapplicable.

From the size of commercially available Si_3N_4 and SiO_2 membranes we envisage lateral dimensions for the testbed of a few 100 μm. For an atmospheric pressure discharge, which we believe would be most suitable for an initial experimental demonstration, the force on the window will be a few mN which the membranes seem to withstand. Assuming moreover a thickness of 1 mm for the wall embracing the testbed and an opening angle of the recess of 120°, the length of the recess' edges will be a few mm. There is thus enough space for the electron beam to be applied with an incident angle of 45°. The setup shown in figure 1 should thus be possible.

The background dielectric functions for the materials are found in the literature. Fitting experimental data to a set of damped harmonic oscillators, the functions can be written in the form [37–41]

$$\varepsilon(\omega) = \varepsilon_\infty + \sum_{i=1}^{i=4} \frac{f_i \omega_i^2}{\omega_i^2 - \omega^2 - \mathrm{i}\gamma_i \omega} \qquad (30)$$

with $\omega_i = 2\pi\nu_i = 2\pi c/\lambda$. The parameters in this equation are given in table 1. In addition to the dielectric functions ε and the electron affinities χ we also need the effective electron masses m_e^* in the conduction bands of the plasma-facing films. In units of the electron mass $m_e^* = 0.4$, 0.5 and 0.24 for Al_2O_3 [50], SiO_2 [51], and ZnO [52], respectively. The temperature is set to $T = 300$ K in all calculations and $\varepsilon_p = \varepsilon_v = 1$.

Within the spectral range where the charge fluctuations whose density dependence we utilize for diagnostic purposes occur, the dielectric functions have to be essentially real. To see that this is the case we plot in figure 3 the dielectric functions for Al_2O_3 and CaO, indicating the fluctuation's energy range by two vertical dashed lines. Clearly, within this band the imaginary parts of the dielectric functions are very small. For SiO_2 and ZnO the situation is the same except that the energy range of interest (as well as the other features in the dielectric function) shifted, respectively, to higher and lower energies.

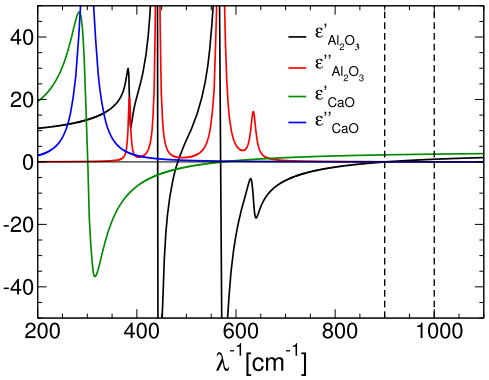

Figure 3. Background dielectric functions for CaO and Al_2O_3 as obtained from (30) using the parameters in table 1. The dashed vertical lines denote the spectral range of the collective excitation of the electrons inside the Al_2O_3 film which we use as a charge diagnostic.

Table 1. Parameters used in (30) for the background dielectric functions of CaO[37], Al_2O_3 [38, 39], SiO_2 [40], and ZnO [41], the materials used in the EELS setup for measuring the wall charge.

	CaO	Al_2O_3	ZnO	SiO_2
ε_∞	3.3856	3.2	3.7	2.356
ε_0	–	9.0	7.8	4.32
ν_1[cm^{-1}]	300	385	406	1227
f_1	9	0.3	4.1	0.009
γ_1 [cm^{-1}]	32	5.58	7.5	134.97
ν_2[cm^{-1}]	–	442	–	1163
f_2	–	2.7	–	0.01
γ_2 [cm^{-1}]	–	4.42	–	6.978
ν_3[cm^{-1}]	–	569	–	1072
f_3	–	3	–	0.67
γ_3 [cm^{-1}]	–	11.38	–	7.6112
ν_4[cm^{-1}]	–	635	–	797
f_4	–	0.3	–	0.11
γ_4 [cm^{-1}]	–	12.7	–	7.173
ν_5[cm^{-1}]	–	–	–	697
f_5	–	–	–	0.018
γ_5 [cm^{-1}]	–	–	–	8.364
ν_6[cm^{-1}]	–	–	–	450
f_6	–	–	–	0.82
γ_6 [cm^{-1}]	–	–	–	4.05
ν_7[cm^{-1}]	–	–	–	394
f_7	–	–	–	0.33
γ_7[cm^{-1}]	–	–	–	2.758

After these material considerations, let us now turn to the Al_2O_3/CaO system. We discuss it in great detail to indicate the reasoning behind the doping strategy and also to give an idea of the kind of charge fluctuation utilized as a charge diagnostic.

Initially we simulated an undoped stack with thickness 40 nm (which we consider sufficient for mechanical stability) and indeed found a loss peak strongly shifting with the density of the surplus electrons accumulated from the plasma and

hence suitable for our purpose. Unfortunately, the intensity of the peak is rather small because it arises from a multipole excitation of the electrons. In units of the strength of the surface (Fuchs–Kliewer) phonon at the vacuum-CaO interface, located at 524 cm^{-1}, which we take as a reference strength, the peak height was only around 10^{-6} for a 10 nm Al_2O_3 film with a plasma-induced surface charge density $n_s^p = 5 \cdot 10^{11}\,cm^{-2}$ on top of a 30 nm CaO layer. Such a faint signal is most probably undetectable by current EELS instrumentation. In a recent application to nanoplasmonics [53], for instance, EELS had a sensitivity of 10^{-4} in units of the elastic peak. Since the Fuchs–Kliewer phonon we use for normalization is typically an order of magnitude weaker than the elastic peak, signals should not be weaker than 10^{-3} in our units in order to be detectable.

Although electron counting techniques may advance [54], thereby pushing the sensitivity limit, we take 10^{-3} as a critical value. Measures are thus necessary to increase the signal strength up to this value. Increasing the signal strength by reducing the thickness of the substrate is not viable because it would threaten the mechanical stability. Another possibility is to increase the density of the electron gas by pre-n-doping the Al_2O_3 film. Due to the pre-doping a loss peak of lower order (and hence higher intensity) becomes charge sensitive and hence suitable for charge diagnostics. It defines also a reference peak, present without surplus electrons from the plasma, which should help calibrating the method. The data presented below are therefore for a doped Al_2O_3 film. Due to the doping the confinement potential is of course no longer simply the potential well arising from the electron affinities. The potential is affected by the Coulomb interaction between the electrons and should be calculated self-consistently [36], but for demonstrating the basic principle of the charge measurement this is not necessary. We leave it thus for the future. The charge accumulation from the plasma itself, however, is not affected by the doping.

After these remarks, let us now turn to the EELS spectrum of a stack with a pre-n-doped plasma-facing Al_2O_3 film. Figure 4 shows data for wavenumbers where the loss is due to a fluctuation of the electron gas in a 10 nm film doped with a bulk electron density $n_b^d = 10^{18}\,cm^{-3}$. In the left panel the loss peak is plotted as a function of the density n_s^p of additional electrons coming from the plasma. Clearly, for a substrate thickness $s = 30$ nm the peak does not have quite the required strength but reducing the substrate thickness a little will push the strength above the critical value, as will be discussed in the next paragraph. How the peak shifts with n_s^p for different substrate thicknesses is plotted in the right panel. Notice the position of the peak for $n_s^p = 0$ depends weakly on s despite the unchanged bulk electron density in the film. We attribute this to a small substrate-induced redistribution of spectral weight due to changes in the electric field producing slightly different loss maxima. For all the chosen values of s the peak shifts nicely with n_s^p and is thus well suited for measuring n_s^p by simply recording the spectral position. Due to the limited energy resolution of EELS [25], only experimental shifts larger than $\Delta\lambda^{-1} = 4\,cm^{-1}$ are detectable. Hence, charge densities $n_s^p > 10^{11}\,cm^{-2}$ may be measurable

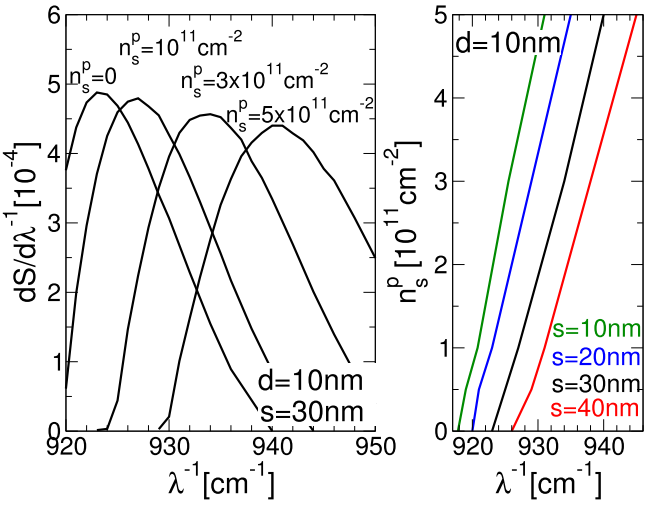

Figure 4. EELS spectra for an Al_2O_3/CaO structure at 300 K in the energy range where the resonance is located we use as a diagnostic for the plasma-induced charges in the Al_2O_3 film. The film's thickness and background doping are, respectively, $d = 10$ nm and $n_b^d = 10^{18}\,cm^{-3}$ corresponding to a surface charge density $n_s^d = n_b^d d = 10^{12}\,cm^{-2}$. Left panel: Loss peak normalized to the strength of the Fuchs–Kliewer phonon of the vacuum-CaO interface as a function of the plasma-induced surface charge density n_s^p [corresponding to a bulk density $n_b^p = n_s^p/d$] for a substrate with thickness $s = 30$ nm. Right panel: Energetic position of the loss peak as a function of n_s^p for four different substrate thicknesses.

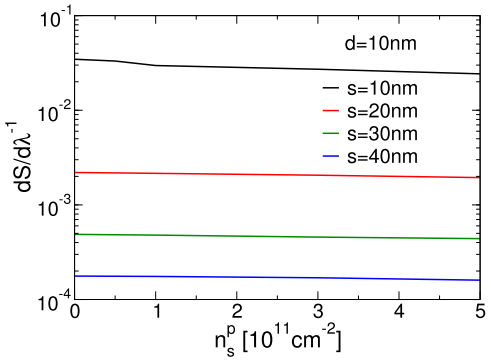

Figure 5. Intensity of the loss peaks shown in figure 4 as a function of n_s^p. The thicker the substrate the weaker the loss peak, as expected. The EELS spectrum is normalized to the intensity of the Fuchs–Kliewer phonon at the vacuum-CaO interface. As explained in the main text, we expect the critical strength below which the signal becomes undetectable to be around 10^{-3} in these units. Hence, the sensitivity of current EELS instrumentation may be not sufficient for substrates thicker than 30 nm.

using this technique. Based on measurements of the wall charge using the Pockels effect [15–19] and experimental studies of the charging of dust particles in low-temperature plasmas [55] this is at the upper limit of the range expected for plasma-facing dielectrics. But inside filaments of atmospheric pressure barrier discharges, surface charges larger than $10^{11}\,cm^{-2}$ are possible [15, 16] as well as in discharges running at sufficiently high current density [56]. For a first experimental realization of the EELS approach these types of discharges would thus be good choices.

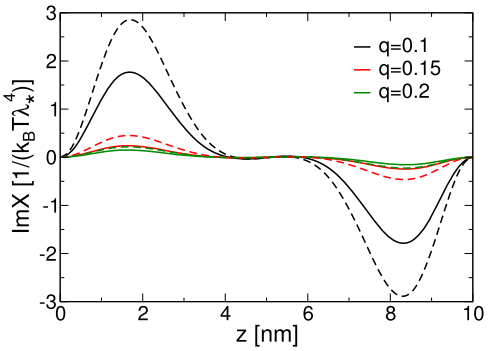

Figure 6. The function $\mathrm{Im}X(q_\parallel, \omega, z)$ for an Al_2O_3/CaO setup with $d = 10$ nm, $s = 30$ nm, $n_b^d = 10^{18}$ cm^{-3} [corresponding to $n_s^d = 10^{12}$ cm^{-2}], and two values for the density of the plasma-induced surplus electrons: $n_s^p = 10^{11}$ cm^{-2} (solid lines) and $n_s^p = 5 \cdot 10^{11}$ cm^{-2} (dashed lines). The lateral momentum $q_\parallel$ in units of $(\lambda_*)^{-1} = 1/\sqrt{\hbar^2/2m_e^* k_B T}$ and the energy $\hbar\omega$ in units of wavenumbers making in each case $P(q_\parallel, \omega)$ maximal are given by (0.1, 927.742 cm^{-1}), (0.15, 923.538 cm^{-1}), and (0.2, 921.318 cm^{-1}) for $n_s^p = 10^{11}$ cm^{-2} and (0.1, 941.837 cm^{-1}), (0.15, 936.1 cm^{-1}), and (0.2, 932.691 cm^{-1}) for $n_s^p = 5 \cdot 10^{11}$ cm^{-2}. For each density the three doubles belong to the domain D over which $P(q_\parallel, \omega)$ has to be integrated according to (1). The z-dependence of $\mathrm{Im}\,X(q_\parallel, \omega, z)$ shows that the charge fluctuation giving rise to the peak in $P(q_\parallel, \omega)$ is a surface plasmon localized close to the boundaries of the Al_2O_3 film.

The strength of the loss peaks is shown in figure 5. According to the considerations presented above we take 10^{-3} as the critical strength in units of the strength of the Fuchs–Kliewer phonon below which the signal cannot be detected anymore. As can be seen, the background doping pushes the signal strength for $s < 30$ nm above this critical value, leaving the system with $s = 30$ nm at the margin. Let us at this point however caution a bit. In the literature EELS data are mostly given in arbitrary units. Our estimate of the critical signal strength is based on one [53] of the few publications where the data are normalized to a particular peak and hence estimable from an intensity point of view. It may be possible that electron detectors used in EELS are in fact more sensitive than we believe. The signal could then by accordingly weaker.

In order to understand the physics of the loss peak we are tracking as a function of n_s^p, we analyzed the spatial structure of the charge fluctuation giving rise to it using the procedure developed by Streight and Mills [34]. They noticed that for ω residing on the loss peak and $q_\parallel$ fixed to a value contributing to the EELS spectrum according to the ellipse equation (4) the $z-$ dependence of the function $\mathrm{Im}X(q_\parallel, \omega, z)$, with $X(q_\parallel, \omega, z)$ defined in (29), reflects the spatial form of the charge fluctuation associated with the peak. Figure 6 shows this function for two different values of n_s^p for a structure with $d = 10$ nm, $s = 30$ nm, and $n_b^d = 10^{18}$ cm^{-3}. The three doubles $(q_\parallel, \hbar\omega)$ are in each case fixed to the value where $P(q_\parallel, \omega)$ is maximal. Since the potential well confining the electrons to the film is, in our crude model infinitely deep, the charge fluctuations are in all cases symmetric with respect to the film center. The fluctuation is maximal close to the boundaries of the film. Hence, it represents a surface plasmon. Increasing the density n_s^p changes mainly the amplitude of the oscillation. The overall structure remains the same. Hence, we are indeed tracking a particular surface plasmon of the film with the density of the surplus electrons coming from the plasma.

Table 2. Comparison of the de Broglie wavelength λ_{dB} and screening length λ_s for an Al_2O_3 film with thickness d and charge density $n_b = n_b^d + n_b^p$, where n_b^d is the film's background electron density due to doping, to be taken in all cases as 10^{18} cm^{-3}, and $n_b^p = n_s^p/d$ the density of the additional electrons coming from the plasma. As can be seen λ_{dB} and λ_s are of the same order. Hence, a nonlocal description of the modification of the film's dielectric function due to the charge carriers is required.

	$\mathbf{Al_2O_3}(\lambda_{\mathrm{dB}} = 9.9$ nm)		
d/nm	$n_s^p[10^{11}$ cm$^{-2}]$	$n_b[10^{18}$ cm$^{-3}]$	λ_s[nm]
5	1	1.2	3.3
10	1	1.1	3.4
15	1	1.07	3.5

The need for using the nonlocal response theory of Mills and coworkers [32–34] can be seen as follows. It is necessary in cases where the screening length $\lambda_s = \sqrt{k_B T/4\pi n_b e^2}$ due to the electrons producing the charge fluctuation the EELS electron couples to is on the same order as the (thermal) de Broglie wavelength $\lambda_{\mathrm{dB}} = \sqrt{(2\pi\hbar)^2/3m_e^* k_B T}$. The density $n_b = n_b^d + n_b^s$ with n_b^d being the bulk electron density due to the background doping and n_b^p the bulk density of the electrons coming from the plasma (corresponding to a surface density $n_s^p = n_b^p d$). As can be seen in table 2, the screening length and de Broglie wavelength, given for three different values of d and an electron density typical for our setup, are of the same order. The nonlocal theory is thus required to describe the dielectric response of the electrons in the film. In fact, the loss peak we are monitoring is even absent in the local theory which uses a simple Drude term added to the film's background dielectric function [21].

Having discussed the Al_2O_3/CaO system at length we now turn to the SiO_2/CaO and the ZnO/CaO systems, demonstrating thereby that the proposal is not restricted to a particular material combination. Instead it is rather flexible as far as the plasma-facing dielectric is concerned. The substrate is critical; it has to be electronegative, which is not a common property. Because of the peculiarity of the from-the-back scattering geometry the CaO substrate and the plasma-facing SiO_2 and ZnO films have to be again sufficiently thin. Pre-doping of the films is also necessary.

In figure 7 we show the loss peaks for 10 nm thick SiO_2 and ZnO films on top of a 30 nm thick CaO substrate. Compared to Al_2O_3, the loss peaks are at different energies but the charge-induced shifts are again large enough to enable charge diagnostics. The strength of the peaks depends on the material via the electron effective mass and the background dielectric function. For the SiO_2/CaO system it is about one order of magnitude smaller than for the Al_2O_3/CaO system whereas for the ZnO/CaO system it is an order of magnitude

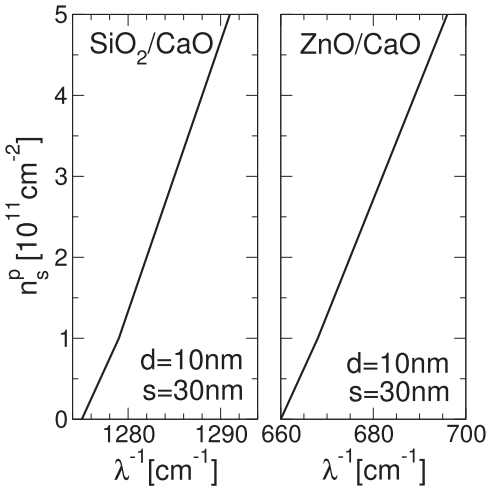

Figure 7. Energetic position of the loss peaks as a function of n_s^p for 10 nm thick SiO_2 and ZnO layers as the plasma-facing films. The substrate is a 30 nm thick CaO layer, the film's background doping is $n_b^d = 10^{18}\,\mathrm{cm}^{-2}$, and the parameters of the probing electron are the same as for the Al_2O_3/CaO system.

larger. From the spectroscopy point of view the latter would thus be ideally suited for an experimental proof of principle.

4. Conclusions

We described an EELS setup for determining the density of electrons accumulated by a plasma-facing electropositive dielectric solid. It is based on a two-layer structure, consisting of a film and a substrate, inserted into an intentionally cut out recess of the wall of the discharge providing the electrons. The film is made out of the material whose plasma-induced charging one wants to know while the substrate ensures the stability of the structure and the confinement of the charges to the film. It is also the layer to which the probing electron beam is applied. The device is geared towards measuring the total charge accumulated by the plasma-facing structure. In principle a structure of this type could also be used to determine the profile of the charge distribution perpendicular to the plasma-solid interface using EELS. It is then however necessary to base the theoretical analysis on a self-consistent kinetic theory of the electric double layer at the plasma-solid interface because otherwise the width of the space charge cannot be determined. In addition the film has to host the whole space charge. How challenging this will be for the EELS sensitivity limit will be shown in future work.

The main goal of this work was to find an EELS setup for measuring the total charge residing inside a plasma-facing dielectric film. For that purpose we made simplifying assumptions and neglected a number of aspects which may be of importance for a quantitative analysis of experimental data. For instance, the plasma in front of the structure is not modelled, it simply provides surplus charges/electrons for the film. Furthermore, the charge confinement is not calculated self-consistently and the charges inside the film are assumed to be thermalized. It is also assumed that all the electrons coming from the plasma are accumulated spatially homogeneously in the film's conduction band, ignoring surface and defect states. These factors will modify the EELS spectrum quantitatively but not qualitatively. The principle of our proposal–confining the wall charge to a narrow film, stabilizing the film using a substrate, and reading-out the charge density from the shift of a loss peak in the from-the-back EELS–is unaffected by them.

To obtain a sufficiently strong loss peak, detectable by current EELS instrumentation, in the peculiar scattering geometry on which our proposal is based, it is most probably necessary to pre-n-dope the plasma-facing film. For the principle of the method the doping is not necessary. Even the undoped film has loss peaks due exclusively to plasma-induced charging but they are rather faint because of their multipole character. However, the pre-doping also has the nice additional effect of providing a reference peak, present also when the plasma is off. Once the plasma is on and the film is flooded by electrons from the plasma the peak shifts with the density of the additional electrons. From the peak position the density can thus be determined. Our results for three different electropositive dielectrics (Al_2O_3, SiO_2, and ZnO) on top of an electronegative CaO layer indicate that from-the-back EELS may indeed work as a charge diagnostics if it is based on sub-100 nm testbeds.

Acknowledgments

In the initial stages this work was supported by the Deutsche Forschungsgemeinschaft through the Transregional Collaborative Research Center SFB/TRR24.

ORCID iDs

F X Bronold https://orcid.org/0000-0001-7802-1387

References

[1] Bronold F X and Fehske H 2017 *J. Phys. D: Appl. Phys.* **50** 294003
[2] Lieberman M A and Lichtenberg A J 2005 *Principles of Plasma Discharges and Materials Processing* (New York: Wiley-Interscience)
[3] Langmuir I and Mott-Smith H 1924 *Gen. Electr. Rev.* **27** 449
[4] Eden J G *et al* 2013 *IEEE Trans. Plasma Sci.* **41** 661
[5] Chen K-F and Eden J G 2008 *Appl. Phys. Lett.* **93** 161501
[6] Tabib-Azar M and Pai P 2017 *Micromachines* **8** 117
[7] Wagner C J, Tchertchian P A and Eden J G 2010 *Appl. Phys. Lett.* **97** 134102
[8] Neyts E C 2016 *Plasma Chem. Plasma P.* **36** 185
[9] Kindel E and Arndt R 1980 *Beitr. Plasmaphysik* **20** 119
[10] Li M, Li C, Zhan H, Xu J and Wang X 2008 *Appl. Phys. Lett.* **92** 031503
[11] Opaits D F, Shneider M N, Miles R B, Likhanskii A V and Macheret S O 2008 *Phys. Plasmas* **15** 073505
[12] Radu I, Bartnikas R and Wertheimer M R 2003 *J. Phys. D: Appl. Phys.* **36** 1284

[13] Pangal K, Firebaugh S L and Sturm J C 1996 *Appl. Phys. Lett.* **69** 1471
[14] Viegas P, Slikboer E, Obrusnik A, Bonaventura Z, Sobota A, Garcia-Caurel E, Guaitella O and Bourdon A 2018 *Plasma Sources Sci. Technol.* **27** 094002
[15] Tschiersch R, Bogaczyk M and Wagner H-E 2014 *J. Phys. D: Appl. Phys.* **47** 365204
[16] Bogaczyk M, Wild R, Stollenwerk L and Wagner H-E 2012 *J. Phys. D: Appl. Phys.* **45** 465202
[17] Gégot F, Callegari T, Aillerie M and Boeuf J P 2008 *J. Phys. D: Appl. Phys.* **41** 135204
[18] Sakurai T, Yoda H, Terayama T, Ishii K and Murakami Y 2007 *Japan. J. Appl. Phys.* **46** 3596
[19] Jeong D C, Bae H S and Whang K W 2005 *J. Appl. Phys.* **97** 013304
[20] Rasek K, Bronold F X and Fehske H 2018 *Europhys. Lett.* **124** 25001
[21] Ibach H and Mills D L 1982 *Electron Energy Loss Spectroscopy and Surface Vibrations* (New York: Academic)
[22] Lambin P, Vigneron J P and Lucas A A 1985 *Phys. Rev.* B **32** 8203
[23] Thiry P A, Liehr M, Pireaux J J and Caudano R 1987 *Phys. Scripta* **35** 368
[24] Ibach H 1994 *Surf. Sci.* **299/300** 116
[25] Rizzi A 1997 *Fresenius J. Anal. Chem.* **358** 15
[26] Lüth H 2015 *Solid Surfaces, Interfaces and Thin Films* (Berlin, Heidelberg: Springer)
[27] Lüth H 1988 *Vacuum* **38** 223
[28] Lüth H 1986 *Surf. Sci.* **168** 773
[29] Ritz A and Lüth H 1984 *Phys. Rev. Lett.* **52** 1242
[30] Lüth H 1983 *Surf. Sci.* **126** 126
[31] Mahboob I, Veal T D, McConville C F, Lu H and Schaff W J 2004 *Phys. Rev. Lett.* **92** 036804
[32] Mills D 1975 *Surf. Sci.* **48** 59
[33] Ehlers D H and Mills D L 1987 *Phys. Rev.* B **36** 1051
[34] Streight S R and Mills D L 1989 *Phys. Rev.* B **40** 10488
[35] Gasiorowicz S 1974 *Quantum Physics* (New York: Wiley)
[36] Streight S R and Mills D L 1988 *Phys. Rev.* B **37** 965
[37] Hofmeister A M, Keppel E and Speck A K 2003 *Mon. Not. R. Astron. Soc.* **345** 16
[38] Palik E D 1985 *Handbook of Optical Constants of Solids* (New York: Academic)
[39] Barker A S 1963 *Phys. Rev.* **132** 1474
[40] Spitzer W G and Kleinman D A 1961 *Phys. Rev.* **121** 1324
[41] Heltemes E C and Swinney H L 1967 *J. Appl. Phys.* **38** 2387
[42] Huang M L, Chang Y C, Chang C H, Lin T D, Kwo J, Wu T B and Hong M 2006 *Appl. Phys. Lett.* **89** 012903
[43] Bersch E, Rangan S, Bartynski R A, Garfunkel E and Vescovo E 2008 *Phys. Rev.* B **78** 085114
[44] Coppa B J, Davis R F and Nemanich R J 2003 *Appl. Phys. Lett.* **82** 400
[45] Stoneham A M and Sangster M J L 1981 *Phil. Mag.* B **43** 609
[46] Tselev A, Velmurugan J, Ievlev A V and Kalinin S V 2016 *ACS Nano* **10** 3562
[47] Tselev A, Fagan J and Kolmakov A 2018 *Appl. Phys. Lett.* **113** 263101
[48] Tai K, Houlahan T J, Eden J G and Dillon S J 2013 *Sci. Rep.* **3** 1325
[49] Tao S X, Theulings A, Smedley J and van der Graaf H 2015 *Diamond Relat. Mater.* **53** 52
[50] Perevalov T V, Shaposhnikov A V, Gritsenko V A, Wong H, Han J H and Kim C W 2007 *JETP Lett.* **85** 165
[51] Ludeke R, Wen H J and Schenk A 1998 *Appl. Phys. Lett.* **73** 1221
[52] Ashkenov N *et al* 2003 *J. Appl. Phys.* **93** 126
[53] Bosman M, Ye E, Tan S F, Nijhuis C A, Yang J K W, Marty R, Mlayah A, Arbouet A, Girard C and Han M-Y 2013 *Sci. Reports* **3** 1312
[54] Hart J L, Lang A C, Leff A C, Longo P, Trevor C, Twesten R D and Taheri M L 2017 *Sci. Rev.* **7** 8243
[55] Khrapak S A *et al* 2005 *Phys. Rev.* E **72** 016406
[56] Lin K-M, Ku C-M and Cheng C-H 2019 *Phys. Plasmas* **26** 013508